



1 Investigating the Mechanism of Typhoon Tracks on Ozone Pollution

2 **Episodes in Guangdong, China**

3

4 Xi Chen¹, Xiaoyang Chen^{2*}, Long Wang¹, Shucheng Chang¹, Minhui Li¹, Chong
5 Shen³, Chenghao Liao¹, Yongbo Zhang¹, Mei Li⁴, Xuemei Wang^{5*}

6

7

8 1. Institute of Atmospheric Environment, Guangdong Provincial Academy of
9 Environmental Science, Guangzhou 510045, China

10 2. Guangzhou Institute of Tropical and Marine Meteorology of China Meteorological
11 Administration, GBA Academy of Meteorological Research, Guangzhou, 510640,
12 China

13 3. Guangzhou Ecological and Agricultural Meteorological Center, Guangzhou, 511430,
14 China

15 4. Institute of Mass Spectrometry and Atmospheric Environment, Guangdong
16 Provincial Engineering Research Center for On-line Source Apportionment System
17 of Air Pollution, Jinan University, Guangzhou 511486, PR China

18 5. Guangdong-Hongkong-Macau Joint Laboratory of Collaborative Innovation for
19 Environmental Quality, College of Environment and Climate Jinan University,
20 Guangzhou 511486, PR China

21

22

23 Corresponding author: Xuemei Wang (eciwxm@jnu.edu.cn), Xiaoyang Chen
24 (chenxiaoyang@gd121.cn)

25

26



27 Key Points:

- Proximal northward-recurving typhoons are the most likely to induce ozone pollution.
- The northward typhoon will cause ozone to increase by 0.3~12.3 ppbv in vertical height.
- The contribution rate of transboundary layer transport under the influence of typhoon to the ozone in the boundary layer can reach 16%.



37

38

39 **Abstract**

40 Ozone (O_3) pollution has emerged as one of the core challenges in atmospheric
41 environmental governance in China, particularly in Guangdong Province. As a crucial
42 weather system during East Asian summers, typhoons exert profound influences on O_3
43 formation, accumulation, and transboundary transport through variations in their
44 tracks and intensities. This study examined 237 historical typhoons occurring in China's
45 coastal waters between 2013-2023, classifying them into three distinct trajectory
46 types using k-means clustering: westward-moving typhoons (Type 1), Distant
47 northward-recurving typhoons (Type2) and Proximal northward-recurving typhoons
48 (Type3). By integrating ground-based observations, reanalysis data, and WRF-CMAQ
49 model simulations to investigate the mechanisms through which typhoon tracks affect
50 ozone pollution in Guangdong Province. The results demonstrate that for Guangdong
51 Province, proximal northward-recurving typhoons induce more extreme
52 meteorological conditions compared to westward-moving and distant northward-
53 moving typhoons. Backward trajectory analysis reveals that northward-moving
54 typhoons significantly enhance vertical downward transport of upper-level ozone,
55 increasing ozone vertical gradients in Guangdong Province, with concentration
56 enhancements of 2.5–11.6 ppbv (Type 2) and 0.3–12.3 ppbv (Type 3). The analysis of
57 consecutive northward-moving typhoons' impact on ozone pollution in Guangdong
58 Province reveals that surface photochemical reactions served as the dominant factor,
59 while vertical downward transport of upper-level ozone acted as a secondary
60 contributor. During this event, vertical transport contributed up to 39.9 ppbv to near-
61 surface (100 m) ozone concentrations, with cross-boundary-layer transport accounting
62 for up to 16% of boundary layer ozone concentrations, demonstrating that typhoon-
63 induced vertical transport significantly enhances boundary layer ozone levels and
64 consequently worsens surface pollution.



65 **Plain Language Summary**

66 It is well established that typhoon tracks exert significant impacts on ozone
67 pollution. However, current research predominantly focuses on individual typhoon
68 case studies or isolated meteorological factors, leaving a gap in comparative analyses
69 of the mechanisms associated with different typhoon pathways. This study categorizes
70 the trajectories of 237 typhoons that occurred over the western Pacific Ocean,
71 specifically investigating the influence mechanisms of westward-moving typhoons
72 (Type1), distant northward-moving typhoons (Type2), and Proximal northward-
73 recurring typhoons (Type3) on ozone pollution in Guangdong Province. The results
74 demonstrate that close-in northward-moving typhoons induce the most favorable
75 conditions for ozone formation and the least favorable atmospheric dispersion
76 conditions in Guangdong, thereby promoting ozone pollution. Additionally,
77 northward-moving typhoons facilitate the subsidence of high-latitude, high-
78 concentration ozone into the boundary layer, leading to elevated ozone levels. Finally,
79 consecutive northward-moving typhoons trigger widespread and persistent ozone
80 pollution across Guangdong. During this process, cross-boundary-layer transport via
81 vertical motion contributes up to 16% of the ozone concentration within the boundary
82 layer, underscoring the substantial impact of northward-moving typhoons on
83 boundary-layer ozone through vertical transport mechanisms.

84 **1 Introduction**

85 Ozone (O_3) pollution has become one of the core challenges in atmospheric
86 environmental governance in China, particularly in the Pearl River Delta region. As a
87 typical secondary pollutant, the formation of O_3 is dually regulated by precursor
88 emissions (NOx and VOCs) and meteorological conditions. (Dou et al., 2024; Gong et
89 al., 2025; Qiu et al., 2025; Yang et al., 2019). In recent years, despite continuous
90 strengthening of anthropogenic emission control measures, the increasing frequency
91 of extreme weather events has significantly amplified the complexity of O_3 pollution.



92 (Chen et al., 2022a; Lu et al., 2024; Wan et al., 2022; Wang et al., 2024a). Among
93 these factors, typhoons, as a crucial weather system during the East Asian summer,
94 exert profound impacts on ozone (O_3) formation, accumulation, and transboundary
95 transport through their track and intensity variations, which significantly modify
96 regional meteorological conditions (e.g., temperature, humidity, wind speed) and
97 atmospheric transport processes. (Chen et al., 2021; Qu et al., 2021; Shen et al., 2023;
98 Wang et al., 2022a).

99 The peripheral subsidence flows of typhoons frequently induce high
100 temperatures, low humidity, and stagnant weather conditions, which enhances
101 photochemical reactions while suppressing pollutant dispersion, consequently leads
102 to localized O_3 accumulation. (Chen et al., 2022b). Simultaneously, the heat stagnation
103 induced by typhoon conditions favors biogenic emissions, with isoprene
104 concentrations potentially doubling, leading to BVOCs contributing up to 10 ppbv to
105 O_3 formation (Xu et al., 2023). Under the combined influence of the western Pacific
106 subtropical high and typhoon peripheral circulation, tropical cyclones facilitate the
107 downward transport of ozone-rich stratospheric air into the lower troposphere. This
108 process leads to the formation of elevated ozone concentrations in the middle
109 boundary layer. Subsequently, the downward transport of residual layer pollutants
110 significantly contributes to the accumulation of ground-level pollutant concentrations
111 during morning hours (Chen et al., 2021; Zhan et al., 2020; Chen et al., 2022c). The
112 approach of typhoons significantly enhances both biogenic emissions and
113 transboundary ozone transport, with observed increases reaching 78.0% and 22.5%,
114 respectively. The abundance of precursors coupled with intensified photochemical
115 reactions more than doubles ozone formation efficiency. (Wang et al., 2022a).
116 Regarding the effect of vertical transport on ozone pollution under typhoon weather,
117 some researchers attribute observed ozone increases primarily to enhanced surface-
118 level photochemical activity (Huang et al., 2021; Jiang et al., 2024; Wang et al., 2025).
119 In this view, upper-level subsidence flows primarily suppress tropospheric ozone



120 dispersion without making significant positive contributions to ozone transport (Ding
121 et al., 2023; Li et al., 2022; Ouyang et al., 2022). Other studies have documented cases
122 where typhoon-induced vertical mixing facilitates downward transport of elevated
123 ozone layers (e.g., through stratospheric intrusions), generating measurable surface
124 ozone enhancements of 10-15 ppbv (Chen et al., 2021).

125 Current research demonstrates that typhoon impacts on ozone pollution exhibit
126 significant path dependence. Westward-moving typhoons induce increased net ozone
127 production in the Pearl River Delta (PRD) core region prior to landfall, followed by a
128 rapid decline to near-zero levels on the landfall day(Ding et al., 2023). During their
129 initial development stage, typhoons enhance ozone production through subsidence-
130 induced meteorological conditions. However, as they approach landfall, associated
131 heavy precipitation and strong winds effectively scavenge pollutants, leading to
132 negative ozone anomalies over the Yangtze River Delta region. These anomalies extend
133 vertically, with maximum ozone reductions of 14-18 ppbv observed at 5 km
134 altitude(Chen et al., 2021). When typhoons track northward across the Taiwan Strait
135 through the low-latitude western Pacific, they trigger sequential regional ozone
136 pollution episodes in both the Yangtze River Delta (YRD) and Pearl River Delta (PRD)
137 regions(Wang et al., 2022b). The northerly peripheral circulation of such typhoons
138 transports precursors from North China and the Yangtze River Delta (YRD) southward,
139 which, when superimposed with local emissions, triggers abrupt ozone concentration
140 increases(Shen et al., 2023). Successive northward-moving typhoons can elevate O₃
141 concentrations by 30% across eastern China while prolonging pollution duration(Wang
142 et al., 2024b). Furthermore, the interaction between typhoons and the subtropical
143 high can form a compound weather system, which exacerbates O₃ pollution intensity
144 and prolongs its duration(Gao et al., 2020; Han et al., 2020a; Qin et al., 2020). However,
145 current research predominantly focuses on individual typhoon cases or isolated
146 meteorological factors(Kumar et al., 2023; Li et al., 2023a; Zhan et al., 2020), leaving
147 significant gaps in comparative analyses of mechanisms associated with different



148 typhoon tracks. Key unresolved questions include: How do typhoons with distinct
149 paths differentially modulate meteorological conditions and regional transport? How
150 do large-scale circulation changes induced by varying typhoon tracks influence the
151 vertical distribution of ozone? These questions demand systematic investigation to
152 advance our understanding of typhoon- O_3 interactions.

153 As a high-frequency typhoon landing region, Guangdong Province exhibits
154 particularly strong correlations between ozone pollution and typhoon activity
155 (Shuping et al., 2022; Yaoyao et al., 2022). Statistical analyses reveal that over 80% of
156 ozone exceedance days during Guangdong's summer-autumn seasons from 2015-
157 2021 were typhoon-associated (Shen et al., 2023). Under climate change scenarios,
158 observed trends of northward-shifting typhoon tracks and intensifying storm strength
159 may further alter regional ozone pollution patterns (Guo and Tan, 2022). Consequently,
160 elucidating the mechanistic links between typhoon paths and ozone pollution holds
161 dual significance: advancing regional atmospheric multipollutant theory while
162 providing scientific foundations for dynamic, precision-based ozone control strategies.

163 This study systematically investigates all typhoons near Guangdong Province from
164 2013 to 2023 by integrating multi-source observational data and numerical
165 simulations. Through comprehensive classification of typhoon tracks, we conduct in-
166 depth analyses of the relationships between meteorological factors, circulation
167 patterns, atmospheric transport, and three-dimensional ozone distribution under
168 different typhoon paths. Specifically, we examine the contribution of upper-level
169 transport to boundary layer ozone concentrations during typical typhoon events. The
170 research aims to elucidate the differential impacts of various typhoon tracks on O_3
171 pollution in Guangdong region, thereby providing scientific support for refined air
172 quality management strategies.

173 **2 Materials and Methods**

174 **2.1 K-means Clustering Analysis**

175 K-means represents one of the most prevalent partition-based clustering



176 methods. The algorithm categorizes n objects into K clusters based on a predefined
177 parameter K , aiming to minimize the within-cluster sum of squares (WCSS) while
178 maximizing the between-cluster sum of squares (BCSS). This ensures high intra-cluster
179 similarity and low inter-cluster similarity. The K-means algorithm has been widely
180 applied in atmospheric trajectory classification studies due to its effectiveness in
181 identifying characteristic transport patterns(Han et al., 2020b; Yufeng et al., 2024; Zhu
182 et al., 2023).

183 In this study, we performed two distinct clustering analyses using the K-means
184 method: typhoon track clustering and atmospheric transport pathway clustering. For
185 typhoon track clustering: 1. Targeted typhoon tracks over the western Pacific Ocean;
186 2. Employed Euclidean distance metric for data point allocation; 3. Determined the
187 optimal K value by identifying the elbow point where the rate of WCSS decrease
188 substantially diminished; 4. Selected $K=3$ as the optimal cluster number, yielding three
189 distinct typhoon track types (Fig.S3). For atmospheric transport pathway clustering: 1.
190 Analyzed 7-day three-dimensional backward trajectories; 2. Classified atmospheric
191 transport channels into four categories (Fig.S4); 3. Implemented similar optimization
192 procedures for cluster determination. The methodology ensures statistically robust
193 classification of both typhoon trajectories and associated air mass transport patterns,
194 providing a quantitative basis for subsequent ozone transport analysis.

195

196 2.2 HYSPLIT Trajectory Model

197 HYSPLIT is a complete system for computing simple air parcel trajectories, as well
198 as complex transport, dispersion, chemical transformation, and deposition simulations.
199 A common application is a back trajectory analysis to determine the origin of air masses
200 and establish source-receptor relationships(Rolph et al., 2017; Stein et al., 2015).

202 This study employs the NOAA HYSPLIT Trajectory Model (https://www.ready.noaa.gov/HYSPLIT_traj.php) to conduct backward trajectory simulations for 237 typhoon



204 s in the Western Pacific region between 2013 and 2023. The meteorological data used
205 is GDAS (1-degree resolution). The source location is set at 113.5°E, 23.6°N, with the
206 backward trajectories initiated at 14:00 (local time) on the day of peak ozone pollutio
207 n during each typhoon event. The backward simulation runs for 168 hours (7 days), w
208 ith trajectory heights set at 500 m, 1000 m, and 2000 m above ground level (AGL).

209

210 2.3 WRF-CMAQ

211 The WRF-CMAQ modeling system was employed to simulate meteorological
212 fields and ozone concentration variations during the typhoon process. The WRF
213 (Weather Research and Forecasting) model version 3.9 was configured with the
214 following parameterizations: Microphysics, WSM6 Scheme; Cumulus
215 Parameterization: Grell-Freitas (GF) Scheme; Radiation: RRTMG Scheme;
216 Boundary Layer: YSU Scheme; Surface Layer: MM5 Similarity Theory; Land
217 Surface: Noah LSM. The large-scale meteorological fields and boundary conditions
218 were derived from NCEP's Global 6-hourly FNL forecast data. The CMAQ (Community
219 Multiscale Air Quality) model version 5.0.2 was implemented with the IPR (integrated
220 process rate) analysis module. The CB05 mechanism was selected for gas-phase
221 chemistry, while the AE6 mechanism was adopted for aerosol chemistry.

222 The modeling system utilized a triple-nested grid configuration (see **Fig.S1**) with
223 Lambert conformal projection centered at 114°E, 28.5°N and two standard parallels at
224 15°N and 40°N. The outermost domain (D01) had a horizontal resolution of 27 km ×
225 27 km, covering China, Southeast Asia and the western Pacific region. The
226 intermediate domain (D02) featured a 9 km × 9 km resolution encompassing South
227 China, while the innermost domain (D03) employed a 3 km × 3 km resolution focusing
228 on Guangdong Province and surrounding cities. The vertical structure consisted of 14
229 layers with the model top set at 200 hPa. For the first and second nested domains, the
230 air pollutant emission inventory adopted was the 0.25°×0.25° MEIC (Multi-resolution
231 Emission Inventory for China) developed by Tsinghua University for the year 2020. For



232 the third (innermost) domain, a higher-resolution 3 km×3 km emission inventory
233 compiled by the research team (Li et al., 2023b) was utilized. The simulation period
234 spanned from 00:00 UTC on 24 August to 00:00 UTC on 31 August 2020.

235 In the present study, O₃ was used as a model pollutant to analyze the effects of
236 atmospheric processes on the pollutants' value in deep convection events by using
237 Integrated Process Rate (IPR) analysis. The IPR analysis in CMAQ can be used to
238 calculate the influence of different atmospheric processes on the values of pollutants,
239 and to quantify the importance of each process in the evolution of the pollutant
240 value(Chen et al., 2018; Chen et al., 2022a). The processes include gas-phase chemistry
241 (CHEM),vertical advection (ZADV), horizontal advection (HADV), vertical diffusion
242 (VDIF), horizontal diffusion (HDIF), dry deposition(DDEP) and cloud processes (CLDS).

243 **3 Data**

244 **3.1 Typhoon track data**

245 The typhoon track data were obtained from the CMA Best Track Dataset
246 (tcdata.typhoon.org.cn) maintained by the Tropical Cyclone Data Center of China
247 Meteorological Administration. This dataset provides 6-hourly positional and intensity
248 records of tropical cyclones in the Northwest Pacific (including the South China Sea,
249 north of the equator and west of 180°E) since 1949, covering all typhoons
250 approaching/making landfall in China, with a spatial resolution of 0.1°×0.1° (Lu et al.,
251 2021; Ying et al., 2014). For this study, we extracted all typhoon track data from
252 January 1, 2013, to December 31, 2023, including temporal, geographical coordinates
253 (longitude and latitude), and intensity information. After interpolating the data, we
254 performed typhoon track classification using the K-means clustering method.

255

256 **3.2 Ozone data**

257 The ground-level ozone monitoring data were obtained from the China National
258 Environmental Monitoring Center (CNEMC). This dataset contains hourly
259 concentrations of SO₂, NO₂, CO, O₃, PM₁₀, and PM_{2.5} from 1,657 monitoring stations



260 across China. For this study, we extracted hourly O₃ data from 105 stations within
261 Guangdong Province (station locations are shown in **Fig.S2**). Following the "Technical
262 Regulation on Ambient Air Quality Index (on trial)" (HJ 663-2013), we calculated the
263 daily maximum 8-hour average ozone concentration (MDA8 O₃). Days with MDA8 O₃
264 concentrations exceeding 160 µg/m³ (approximately 75 ppbv) were identified as ozone
265 exceedance days.

266 The TROPESS Chemical Reanalysis O₃ Increment 6-Hourly 3-dimensional Product
267 V1 dataset from NASA was utilized to investigate the three-dimensional spatial
268 distribution of ozone under typhoon conditions
269 (https://disc.gsfc.nasa.gov/datasets/TRPSCRO3I6H3D_1/summary). The data are part
270 of the Tropospheric Chemical Reanalysis v2 (TCR-2) for the period 2005-2021. TCR-2
271 uses JPL's Multi-mOdel Multi-cOnstituent Chemical (MOMO-Chem) data assimilation
272 framework that simultaneously optimizes both concentrations and emissions of
273 multiple species from multiple satellite sensors. The data files contains a year of data
274 at 6-hourly resolution, and a spatial resolution of 1.125 x 1.125 degrees at 27 pressure
275 levels between 1000 and 60 hPa. This study extracted data from January 1, 2013 to
276 December 31, 2021 for spatial analysis of ozone distribution.

277

278 3.4 Meteorological data

279 Meteorological data from ERA5 (the fifth-generation European Mesoscale
280 Weather Forecasting Center reanalysis of global climate and weather for the past four
281 to seven decades) was also adopted in order to understand the pollution
282 characteristics. The temporal resolution of the data is hourly and the spatial resolution
283 is 0.25° x 0.25°. The parameters extracted herein include 2-m temperature, surface
284 relative humidity, total cloud cover, downward UV radiation at the surface, total
285 precipitation, mean sea level pressure, the u-component and v-component of wind at
286 the 10m, 175hPa and 900hPa level, boundary layer height, vertical velocity at the 850
287 hPa level, the Geopotential at the 175hPa and 900hPa level.



288 <https://cds.climate.copernicus.eu/cdsapp#!/dataset/reanalysis-era5-single-levels?tab=overview>).

290

291 3.5 ground-level ozone reanalysis dataset

292 The ground-level MDA8 O₃ concentrations across China were obtained from the
293 China 1km High-Resolution Daily Ground-Level Ozone (O₃) Dataset (2000–2023), a
294 high-resolution (1 km) product developed by Wei et al. and hosted on the National
295 Earth System Science Data Sharing Platform (<http://geodata.nnu.edu.cn>) (Wei et al.,
296 2022). This dataset was generated through an ensemble learning approach combining
297 multi-source data, including hourly O₃ measurements from ~940 to 1,630 monitoring
298 stations (2013–2020) under China's Ministry of Ecology and Environment (MEE)
299 network, OMI/Aura total-column O₃ and tropospheric NO₂ retrievals, downward solar
300 radiation (DSR) and surface air temperature (TEM) from ERA5 reanalysis (0.1°
301 resolution), emissions of NO_x, VOCs, and CO from MEIC inventory, land cover from
302 MODIS, elevation from SRTM, and population density from LandScan. The subset of
303 data from January 1, 2013, to December 31, 2023, was temporally aligned with
304 recorded typhoon tracks to assess the spatio-temporal variability of O₃ during periods
305 with distinct typhoon track types.

306 **4 Results**

307 4.1 Characteristics of ozone pollution under different typhoon paths

308 4.1.1 Typhoon track clustering

309 Through k-means clustering analysis, the 237 typhoon tracks over the western
310 Pacific from 2013 to 2023 were classified into three distinct types (**Fig1.a-c**). Type 1
311 comprises typhoons that form in the western Pacific, move into the South China Sea,
312 and subsequently make landfall in South China or pass through its southern maritime
313 areas (total: 105 cases). Type 2 consists of typhoons originating from low-latitude
314 regions of the western Pacific that approach China before recurring northward,



315 traversing Japan and Korea before returning to the western Pacific basin (total: 77
316 cases). Type 3 represents typhoons generated in low-latitude western Pacific regions
317 that approach China and recurve northward, ultimately making landfall in China or
318 dissipating near Japan/Korea (total: 55 cases).

319 For clarity, these three typhoon types are respectively designated as: Type 1:
320 Westward-moving typhoons; Type 2: Distant northward-recurving typhoons; Type 3:
321 Proximal northward-recurving typhoons. Temporal distribution analysis (**Fig1.d**)
322 reveals that both Type 1 and Type 2 primarily occur from July to November, with peak
323 frequency in autumn, while Type 3 is predominantly observed from July to September,
324 showing maximum occurrence during summer.

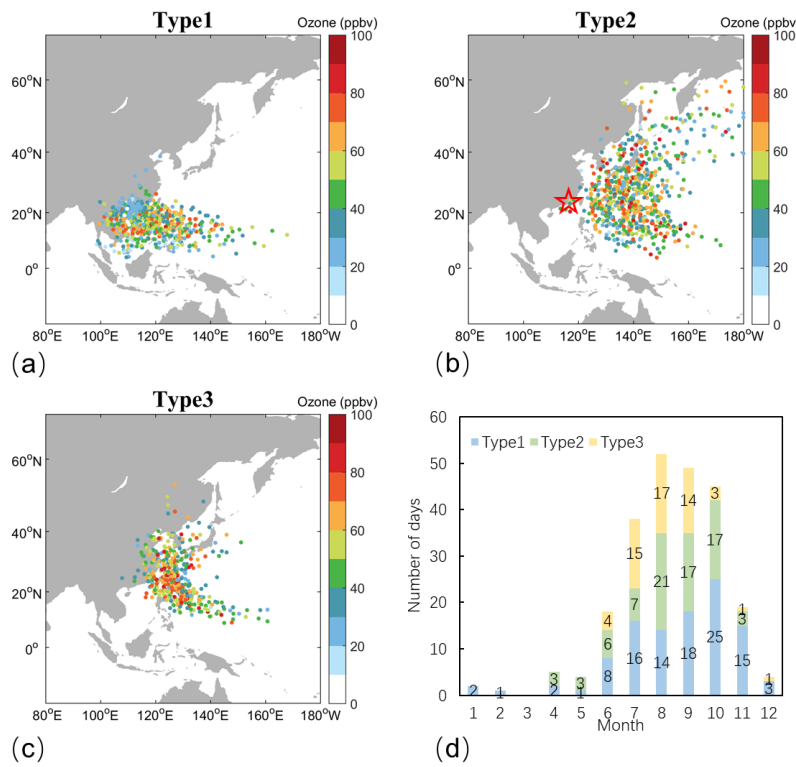
325 4.1.2 Characteristics of ozone pollution

326 Figures 1a-1c illustrate the temporal evolution of maximum daily 8-hour average
327 ozone (MDA8) concentrations in Guangdong Province in relation to typhoon track
328 movements. From the perspective of ozone pollution characteristics, during the
329 approach of Type 1 typhoons toward mainland China, ozone concentrations in
330 Guangdong Province exhibit a gradual increase. If the typhoon does not make landfall,
331 ozone concentrations remain elevated until the typhoon dissipates. However, if the
332 typhoon makes landfall, ozone concentrations decrease rapidly due to precipitation
333 and strong winds (**Fig. 1a**). Recent studies highlight the dual effects of typhoons on
334 ozone: initial stages often enhance ozone through photochemical processes and
335 stratospheric intrusions, whereas landfall phases suppress it via convective activity and
336 precipitation(Chen et al., 2021; Li et al., 2021). Typhoons of Type2 can induce ozone
337 concentration increases in Guangdong Province through long-distance influences, as
338 demonstrated by cases where northward-moving typhoons beyond 40°N still triggered
339 ozone elevation in Guangdong (**Fig.1b**). This phenomenon may be associated with
340 large-scale transport of ozone and its precursors. Typhoons of Type3 tend to induce
341 ozone pollution in Guangdong when approaching eastern China, with peak
342 ozone concentrations occurring when the typhoon reaches approximately 25°N



343 latitude. Following typhoon landfall or eastward deflection, ozone
344 concentrations decrease (**Fig. 1c**).

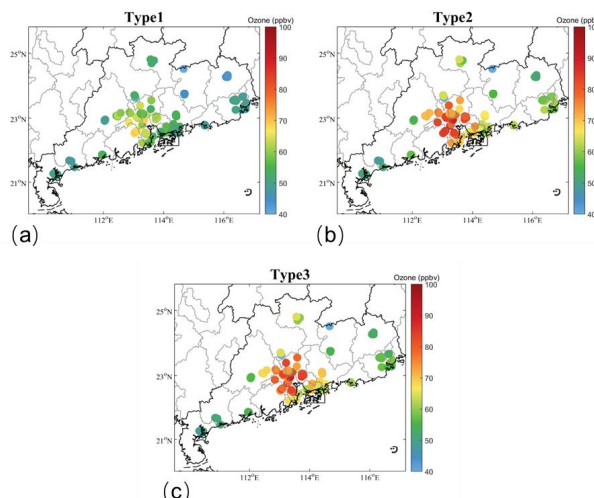
345 We extracted the MDA8 O₃ concentrations during each typhoon event and
346 calculated Type-specific averages to examine ozone distribution patterns in
347 Guangdong under different typhoon types (**Fig. 2**). The results demonstrate that: Type
348 1 corresponds to MDA8 O₃ concentrations ranging 9.2-70.9 ppbv, with an average of
349 20 monitoring stations exceeding standards. Type 2 shows MDA8 O₃ concentrations of
350 12.2-90.3 ppbv, averaging 34 exceedance stations. Type 3 exhibits MDA8 O₃
351 concentrations of 3.3-89.7 ppbv, with 35 stations exceeding limits on average. The
352 spatial analysis reveals that ozone hotspots for all types consistently cluster in central
353 Guangdong, indicating similar spatial distribution patterns despite varying intensity.
354 Type3 exhibited the highest number of non-compliant monitoring sites, while Type1
355 showed the lowest count.



356



357 Figure 1. (a-c) Maximum daily 8-hour average (MDA8) ozone concentrations in Guangdong
358 Province (marked by red pentagrams) under different typhoon tracks(Different colors of dots
359 represent the average ozone concentration at all monitoring stations in Guangdong Province
360 when the typhoon is at that location), and (d) the corresponding temporal distributions of
361 typhoon occurrences for each track type.



362 Figure. 2 Distribution of ozone pollution under different typhoon paths

364 4.1.3 Meteorological characteristics

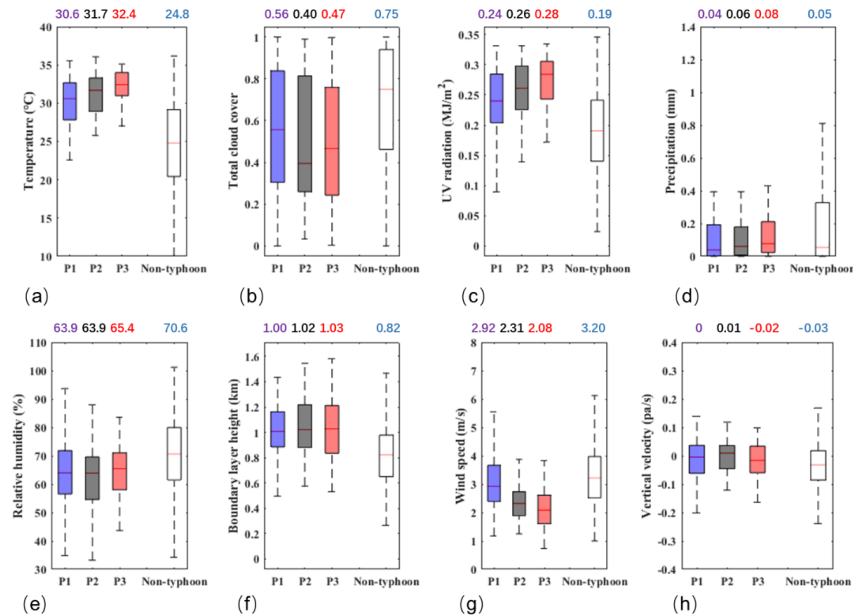
365 To investigate the influence of meteorological factors on ozone pollution in
366 Guangdong Province under different typhoon tracks, we compared the differences in
367 meteorological conditions between three types of typhoon weather and non-typhoon
368 weather in Guangdong. Typhoon conditions refer to the day with the most severe
369 pollution during the typhoon event, while non-typhoon conditions correspond to the
370 remaining periods after excluding the entire typhoon process. The meteorological
371 factors analyzed included surface temperature, total cloud cover, surface solar
372 radiation, precipitation, surface relative humidity, boundary layer height, 10m wind
373 speed, and vertical velocity at 850 hPa. All meteorological data were extracted from
374 ERA5 at 14:00 local time for comparative analysis.

375 The results indicate that, compared to non-typhoon weather, typhoon weather
376 in Guangdong is characterized by higher temperatures, stronger solar radiation, lower
377 cloud cover, reduced precipitation, lower relative humidity, higher boundary layer



378 height, weaker surface winds, and suppressed vertical motion (**Fig.3**). The peripheral
379 circulation of typhoons modifies the thermodynamic and dynamic structure of the
380 boundary layer, creating an "ideal reactor" for ozone formation. Near-surface
381 conditions of high temperatures, low humidity, and weak winds foster a stable
382 boundary layer structure, significantly enhancing photochemical reaction rates (Ding
383 et al., 2023). Additionally, increased solar radiation and elevated boundary layer height
384 further expand the spatial domain for ozone production.

385 A comparison of meteorological characteristics across different typhoon track
386 types reveals that Type 3 corresponds to what may be termed "extreme"
387 meteorological conditions. It brings high temperature(32.4°C), high radiation
388 (0.28MJ/m²), low cloud cover (0.47), low precipitation (0.08mm), low relative humidity
389 (65.4%), high boundary layer height (1.03km), low wind speed(2.08m/s), and less
390 vertical movement (-0.02pa/s) meteorological conditions, which are more likely to
391 cause ozone pollution in Guangdong Province. Compared to non-typhoon conditions,
392 Type 3 exhibits a temperature increase of 7.6°C, a cloud cover reduction of 0.28, a
393 radiation intensity enhancement of 0.09 MJ/m², and a boundary layer height elevation
394 of 0.21 km. It demonstrates the poorest horizontal diffusion conditions, with a near-
395 surface wind speed of 1.12 m/s lower than non-typhoon conditions. The severe ozone
396 pollution observed in Guangdong Province results from the combined effects of strong
397 ozone production rates and poor diffusion conditions, creating a synergistic
398 amplification of pollution levels. The photochemical reaction conditions in Type2 are
399 slightly weaker than those in Type3; however, reduced precipitation inhibits the wet
400 scavenging of ozone and its precursors. Additionally, strong subsidence at the 850 hPa
401 level not only suppresses the vertical diffusion of pollutants within the boundary layer
402 but also transports ozone from higher altitudes downward, further increasing surface
403 ozone concentrations. Compared to the other two typhoon types, Type1 exhibits
404 weaker ozone formation conditions and better dispersion, resulting in the least severe
405 ozone pollution.



406
407 Figure 3. Comparison of meteorological conditions between typhoon and non-typhoon weather.
408 (a–f) represent 2m temperature, total cloud cover, surface solar radiation, precipitation,
409 relative humidity, boundary layer height, 10m wind speed, and vertical velocity at 850 hPa, respectively.
410 P1, P2, and P3 denote three distinct typhoon tracks, while Non-typhoon refers to non-typhoon
411 conditions. The numerical values above each boxplot indicate the median of the corresponding
412 dataset.

413 4.2 Effect of regional transport on ozone distribution

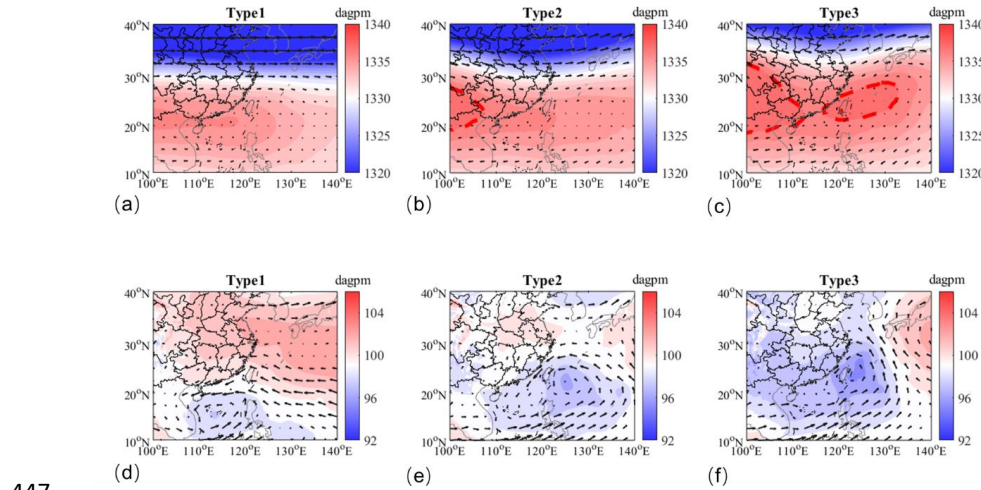
414 4.2.1 Three-dimensional spatial distribution of ozone

415 The impact of typhoons on ozone extends beyond creating favorable
416 photochemical conditions. The regional transport induced by large-scale circulation
417 plays a pivotal role in determining ozone concentration distribution(Chen et al., 2022b;
418 Wang et al., 2018). Typhoon tracks modify regional airflow patterns, facilitating cross-
419 regional transport of ozone and its precursors(Chen et al., 2021). This study employs
420 three-dimensional reanalysis O₃ data (2013-2021) coupled with wind fields and
421 geopotential height to examine how typhoon-induced regional transport affects the
422 three-dimensional spatial distribution of ozone concentrations (**Fig4-5**). When the
423 typhoon moves northward (type 2 and type3), a high-pressure center emerges over



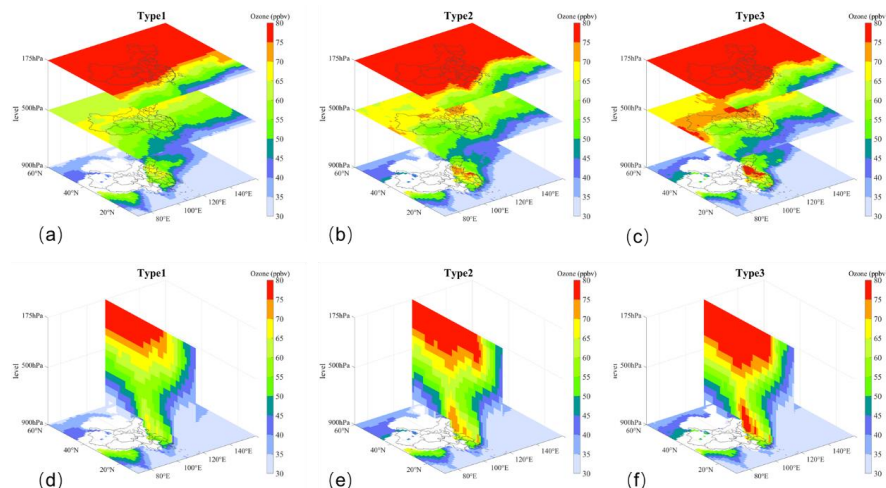
424 western China at the 175 hPa level, causing a southward displacement of the westerly
425 jet. Under this circulation pattern, an ozone transport pathway is established,
426 extending from high to low latitudes and accompanied by subsidence (**Fig. 4b, c**).
427 Through this transport channel, stratospheric ozone with high concentrations (>75
428 ppbv) is advected southward to approximately 20°N and descends below the 500 hPa
429 level (**Fig. 5e, f**). Mechanistic analysis demonstrates that the combined effects of the
430 westerly jet and mid-latitude high-pressure systems on typhoon motion create upper-
431 tropospheric wind convergence, which enhances stratosphere-to-boundary-layer
432 transport of ozone-rich air from the North China Plain (Meng et al., 2022). In contrast,
433 westward-propagating typhoons (Type 1) do not generate perturbations in the
434 westerly jet, and no pronounced southward transport or subsidence of upper-level
435 ozone is evident (**Fig. 5a, d**).

436 As demonstrated by recent studies (Wang et al., 2022b; Yufeng et al., 2024), the
437 peripheral circulation of western North Pacific typhoons can effectively transport
438 ozone and its precursors from source regions (including the Yangtze River Delta, Fujian,
439 and Anhui provinces) to Guangdong through well-organized atmospheric transport
440 pathways. Analysis of ozone distribution at the 900 hPa level reveals that northward-
441 moving typhoons not only induce ozone pollution in Guangdong, but also lead to
442 elevated ozone concentrations in the Beijing-Tianjin-Hebei and Yangtze River Delta
443 regions (**Fig. 5b,c**). During the typhoon's northward progression, the low-pressure
444 center traverses China's eastern coastal areas, where cyclonic circulation facilitates
445 southward transport of pollutants along the coast, ultimately impacting Guangdong
446 Province (**Fig. 4e,f**).



447

448 Figure 4. Comparison of circulation patterns under different typhoon tracks. (a-c) show
449 geopotential height and wind fields at 175 hPa (upper panels) and 900 hPa (lower panels),
450 respectively. The red curves indicate the positions of high-pressure centers.



451

452 Figure 5. Three-dimensional spatial distribution of ozone under different typhoon tracks. (a-c)
453 Horizontal ozone distributions at 900 hPa, 500 hPa, and 175 hPa for the three typhoon track
454 types. (d-f) Horizontal ozone distributions at 900 hPa and corresponding vertical cross-sections
455 along 114°E for each typhoon type.

456

457 Figure S5 presents the spatial distribution of ground-level MDA8 O₃
458 concentrations across China, as derived from the reanalysis 1 km high-resolution daily
459 dataset, under three distinct typhoon track types (type 1, type 2, and type 3). The



460 analysis focuses on typhoon events, characterized as the date with the highest number
461 of ground monitoring sites exceeding the $160 \mu\text{g}/\text{m}^3$ (~75 ppbv) MDA8 O_3 threshold
462 during the entire typhoon track.

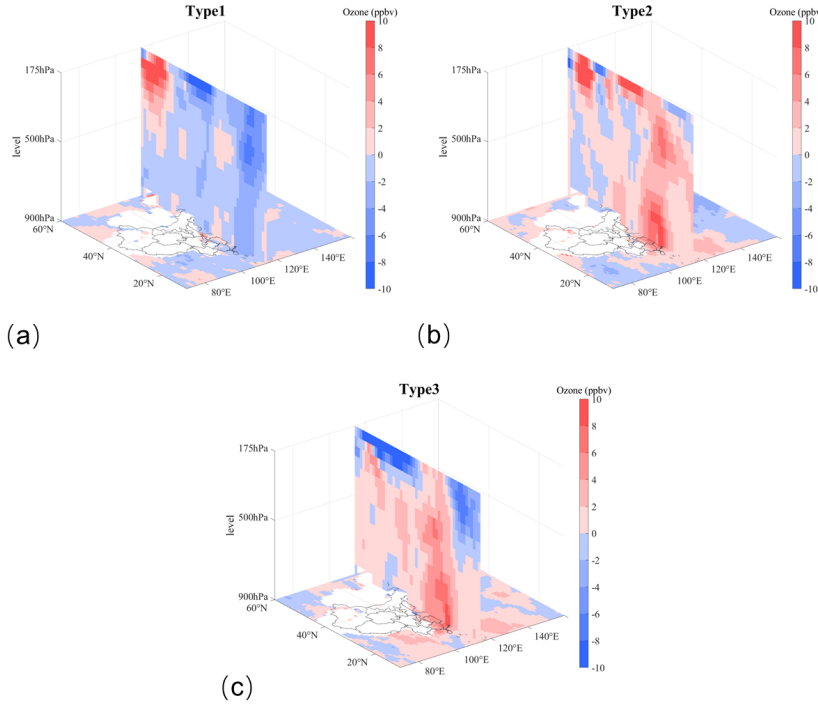
463 Being consistent with spatial distribution of ground monitoring O_3 concentrations
464 in section 4.1.2, here reveals significant spatial heterogeneity in O_3 concentrations
465 across typhoon track types, particularly in Guangdong Province, where the mean
466 MDA8 O_3 follows the order: Type 2 (56.9 ppbv) > Type 3 (54.6 ppbv) > Type 1 (51.25
467 ppbv). This variability is attributed to differences in regional transport pathways and
468 precursor availability. Specifically, type 2 typhoons exhibit elevated O_3 levels in eastern
469 China but reduced concentrations in northern and central regions compared to type 3.
470 The enhanced O_3 under type 2 conditions is driven by two synergistic mechanisms: (1)
471 intensified low-tropospheric transport along China's eastern coastal region, as
472 evidenced by atmospheric circulation patterns (**Fig. 4e**), and (2) the advection of O_3 -
473 rich air masses from northern and central China, which supply abundant precursors to
474 Guangdong, particularly its eastern sector. Type 3 typhoons facilitate a more direct,
475 meridional transport of O_3 from northern and central China, coupled with pronounced
476 stratospheric intrusions that enhance upper-tropospheric O_3 contributions (**Fig. 5c and**
477 **5f**). While type 2 systems lack the robust northern transport pathway observed in type
478 3, they compensate via secondary O_3 delivery through coastal advection, which
479 subsequently propagates inland. This dual transport mechanism culminates in the
480 highest O_3 concentrations in Guangdong, especially the eastern and coastal part,
481 during type 2 events.

482 Collectively, integrating atmospheric dynamics (**Fig.4**), three dimensional
483 evolution of O_3 (**Fig.5**), and ground-level O_3 distributions (**Fig.S5**), underscores the
484 critical role of typhoon-track-dependent transport pathways in modulating regional O_3
485 pollution. These highlight the necessity of considering multi-scale meteorological
486 processes in air quality forecasting and quantifying their contributions to O_3
487 concentrations across different vertical levels.



488 To further investigate typhoon-induced ozone variations, spatial ozone
489 concentration differences between typhoon conditions and non-typhoon conditions
490 (June-November) were calculated (**Fig.6**). The June-November period was selected to
491 eliminate seasonal influences. The results indicate that northward-moving typhoons
492 (Type 2 and Type 3) can induce substantial ozone increases throughout the vertical
493 column (200-900 hPa) (**Fig. 6b,c**). At the central point (113.23°E, 23.16°N), ozone
494 concentration changes ranged between 2.5-11.6 ppbv (Type 2) and 0.3-12.3 ppbv
495 (Type 3). In contrast, Type 1 did not cause significant high-altitude ozone increases,
496 with central point ozone concentration changes ranging from -3.2 to 0.99 ppbv. Studies
497 indicate that when gravity waves break in the upper troposphere and lower
498 stratosphere on the western side of typhoon centers, intense turbulence occurs,
499 leading to stratosphere-troposphere exchange (STE) (Huang et al., 2024). Subsequently,
500 typhoons approaching landfall significantly enhance cross-regional ozone transport
501 from North China to South China through STE (Wang et al., 2024c). This suggests that
502 after Types 2 and 3 typhoons move northward, their cyclonic circulations transport
503 high-concentration ozone from the tropopause to lower latitudes and altitudes
504 through STE, causing significant changes in ozone vertical distribution and increased
505 ozone concentrations within the boundary layer.

506



507
508
509
510
511

Figure 6. Ozone concentration changes induced by different typhoon types (a-c: horizontal distribution changes at 900 hPa and vertical cross-section changes along 114°E for each typhoon track type respectively).

512 4.2.2 Boundary layer ozone

513 To investigate the ozone transport pathways within the boundary layer over
514 Guangdong Province under typhoon conditions, and to examine the differences in
515 ozone sources associated with distinct typhoon tracks, this study conducted HYSPLIT
516 backward trajectory analysis for 237 typhoon events. The analysis focused on 7-day air
517 mass origins at 500m altitude over central Guangdong (Fig.S6). For each typhoon type,
518 cluster analysis of air mass origins was performed. After K-value screening, the air mass
519 origins were classified into four trajectory clusters (Fig.7). Table S1 presents statistics
520 for each trajectory type, including: (1) The percentage of different trajectories, (2)
521 mean ozone concentrations along trajectories, and (3) corresponding surface ozone
522 concentrations.

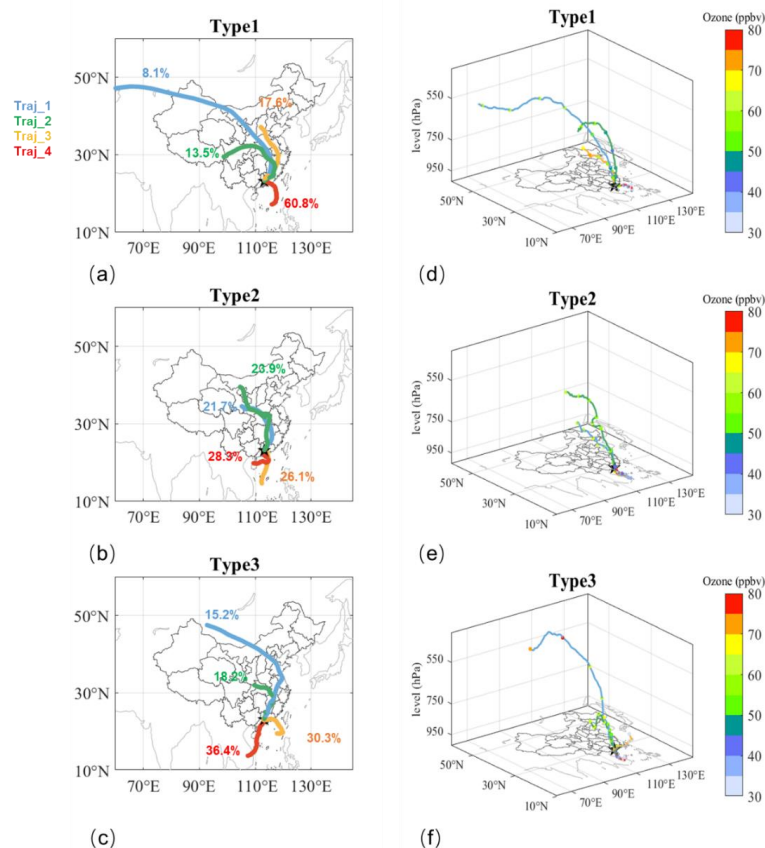


523 Under Type 1 conditions, air masses in the target area mainly originated from
524 within the boundary layer, accounting for 60.8%, with air transported from the South
525 China Sea below 841 meters to Guangdong Province (Traj_4). Analysis of the
526 subtropical high's influence shows that under this typhoon type, Guangdong
527 experienced the highest surface pressure and was closest to the subtropical high
528 (**Fig.S7**). Research indicates that under the influence of the subtropical high, O₃
529 pollution is primarily affected by local emissions (Chen et al., 2024). This aligns with
530 Traj_4's characteristics of short transport distance and low altitude. The other three
531 trajectories originated from northwest China (Traj_1, 8.1%), western China (Traj_2,
532 13.5%), and central China (Traj_3, 17.6%) respectively (**Fig.7a**). The trajectory with the
533 highest surface ozone concentration was Traj_2, which descended from 3794.1 meters
534 with an average ozone concentration of 50.3 ppbv along the trajectory (**Fig.7d**,
535 **Table.S1**). Under Type 2 conditions, nearly half of the air masses in the target area
536 originated from northwest China (Traj_1, 21.7% and Traj_2, 23.9%), while the other
537 half came from the South China Sea region (Traj_3, 26.1% and Traj_4, 28.9%) (**Fig.7b**).
538 Among these, Traj_1 and Traj_2 air masses descended from above 2000m, whereas
539 Traj_3 and Traj_4 air masses were transported within the boundary layer (**Fig.7b**). The
540 trajectory with the highest surface concentration was Traj_1, which descended from
541 2646 meters with an average ozone concentration of 61.9 ppbv along the trajectory
542 (**Fig.7e, Table.S1**). Under Type 3 conditions, Traj_1 carried high-concentration ozone
543 (>75 ppbv) from high-altitude (6356m) over high-latitude areas through North China
544 to the target region, corresponding to the highest surface ozone concentration (15.2%
545 proportion) (**Fig.7f, Table.S1**). The other three trajectories originated from central
546 China (Traj_2, 18.2%) and the South China Sea region (Traj_3, 30.3% and Traj_4,
547 36.4%) (**Fig.7c**).

548 A comparative analysis of air mass trajectories from different directions
549 demonstrates that marine air masses originating from the South China Sea are
550 characterized by lower altitudes and extended residence time over Guangdong



551 Province, thereby constituting local ozone pollution sources. Conversely, continental
552 air masses exhibit longer transport pathways and higher altitudes, representing
553 regional ozone transport sources. Quantitative analysis reveals that the proportional
554 contributions of local pollution sources under different typhoon tracks are 60.8%,
555 55.0%, and 66.4%, respectively. Analysis of long-range transport trajectories reveals
556 that different typhoon types can respectively deliver ozone from maximum altitudes
557 of 7,468 meters (~380 hPa), 8,927 meters (~320 hPa), and 9,980 meters (~250 hPa)
558 into the boundary layer. Type 2 and Type 3 exhibit significantly greater proportion from
559 upper-level air mass transport (23.9% and 15.2% respectively) compared to Type 1.
560 These typhoons can transport ozone from altitudes down into the boundary layer.
561 Combined with the high ozone concentrations along the atmospheric transport
562 pathways, this results in boundary-layer ozone increases of 10.7 ppbv and 12.3 ppbv
563 for these two types, respectively (**Fig6.b-c**).
564
565



566

567 Figure 7. Comparison of boundary-layer air mass trajectory sources under different typhoon
568 tracks: (a-c) two-dimensional views with trajectory percentages indicated numerically; (d-f) three-
569 dimensional views showing ozone concentrations (ppbv) along trajectories (marked by colored
570 points); target regions are denoted by black pentagrams on maps.

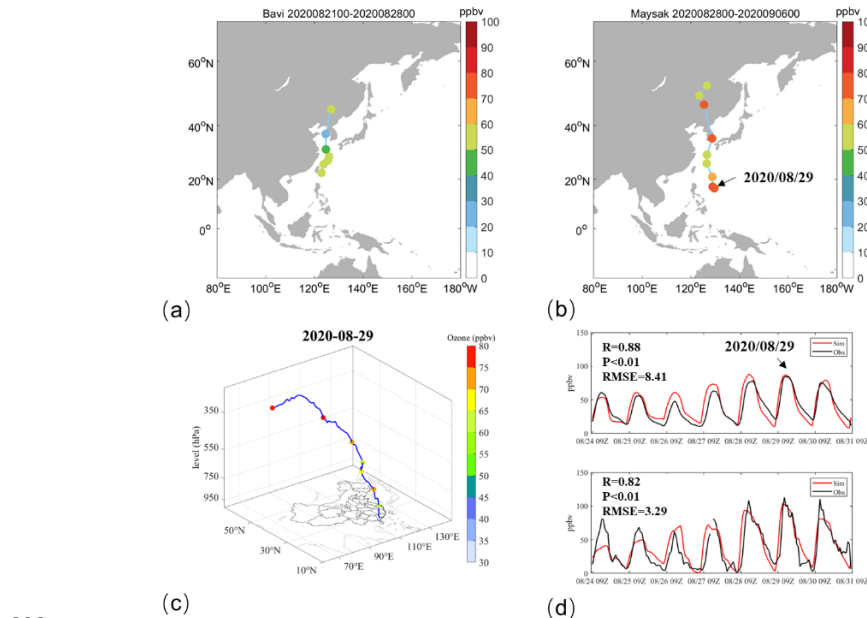
571 4.3 Contribution of typhoons to the vertical transport of ozone

572 During the period from August 21 to September 6, 2020, the consecutive
573 occurrence of two northward-moving typhoons (Bavi and Maysak) triggered
574 prolonged ozone pollution episodes in the Beijing-Tianjin-Hebei and Yangtze River
575 Delta regions, with over 50% of monitoring stations exceeding ozone standards(Cong
576 et al., 2024; Hu et al., 2024). Our study reveals that Guangdong Province similarly
577 experienced extended ozone pollution episodes, particularly between August 28-30



578 and September 1-3, when more than 40 out of 105 monitoring stations (38.1%)
579 recorded exceedances. The most severe pollution occurred on August 29, with 57
580 stations (54.3%) exceeding standards and an average MDA8 ozone concentration of
581 80.6 ppbv (**Fig.8a-b**). Backward trajectory analysis for August 29 identified a 7-day
582 vertical transport pathway from upper levels to the boundary layer, suggesting
583 potential downward mixing of high-ozone air masses (**Fig.8c**). This section examines
584 the period from August 24 to August 31, 2020, employing the WRF-CMAQ model to
585 simulate the spatial distribution of ozone. Integrated Process Rate (IPR) analysis is
586 applied to investigate the formation mechanisms of surface ozone pollution in
587 Guangdong Province under the influence of consecutive northward-moving typhoons,
588 with a quantitative assessment of the impact of vertical transport on ozone
589 concentrations within the planetary boundary layer.

590 The WRF-CMAQ model was used to simulate ozone variations in Guangdong
591 Province from August 24 to 31, 2020, with evaluation results showing excellent
592 performance (**Fig.8d**). For all 105 monitoring stations across the province, the
593 correlation coefficient between observed and simulated ozone concentrations
594 reached 0.88 ($p<0.01$), with a root mean square error (RMSE) of 8.41 ppbv. Focusing
595 on the Sanshui station (112.8°E, 23.15°N), which exhibited both high ozone levels and
596 a clear increasing trend, the correlation coefficient was 0.82 ($p<0.01$) with an RMSE of
597 3.29 ppbv. These results demonstrate that the WRF-CMAQ model successfully
598 captured the spatial distribution and temporal evolution of this ozone pollution event
599 in Guangdong, with statistical metrics meeting operational air quality modeling
600 standards. The model's strong performance, particularly in reproducing both regional
601 patterns and local pollution trends, provides reliable support for subsequent analysis
602 of ozone formation mechanisms under typhoon conditions.



603

604 Figure 8. Consecutive northward-moving typhoon tracks, backward trajectories, and ozone
605 variations. (a-b) Typhoon paths with corresponding MDA8 ozone concentrations in Guangdong
606 province; (c) Backward trajectories at 1300 LST on August 29, 2020; (d) WRF-CMAQ simulated
607 ozone variations (upper panel: average across 105 Guangdong monitoring stations; lower panel:
608 Foshan Sanshui station (112.8°E, 23.15°N) observations, with red lines indicating simulated values
609 and black lines representing monitored concentrations).

610

611 From August 24 to 27, Typhoon Bavi was located along the eastern coastal region
612 of China, moving northward before gradually dissipating. From August 28 to 31,
613 Typhoon Maysak emerged in the South China Sea and progressively approached the
614 Chinese mainland. During this period, we analyzed variations in surface ozone
615 concentrations and their vertical distribution under the influence of these consecutive
616 northward-moving typhoons, based on model simulation results (Fig.9). The results
617 show that the variation in surface ozone distribution can be divided into two stages:
618 The first stage occurred under the influence of Typhoon Bavi, when surface ozone
619 concentrations rapidly increased in the Beijing-Tianjin-Hebei region, Yangtze River
620 Delta, and Pearl River Delta, and was rapidly transported to southwestern China by
621 circulation. The second stage occurred under the influence of Typhoon Maysak, when

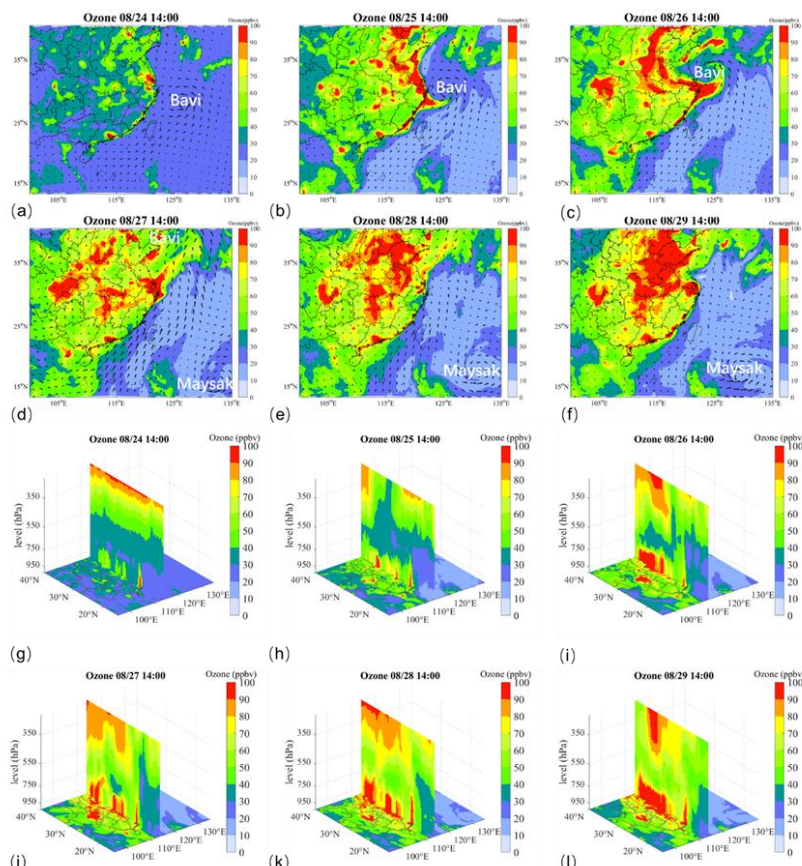


622 ozone concentrations continued to rise across most regions of China. Compared with
623 the first stage, horizontal ozone transport was not significant during the second stage
624 (**Fig. 9a-f**). In the vertical dimension, the consecutive northward-moving typhoons
625 triggered a sustained downward transport process of ozone. Beginning on August 25,
626 downward ozone transport was observed in the upper atmosphere between 35°N and
627 40°N. From August 26 to 29, the zone of ozone subsidence gradually expanded
628 southward, leading to a significant increase in ozone concentrations over Guangdong
629 Province (**Fig. 9g-l**).

630 The IPR process analysis results elucidate the impacts of photochemical reactions
631 and atmospheric transport on ozone concentration variations during this event (**Figs.**
632 **S8-S9**). The photochemical reactions correspond to the CHEM contribution in the
633 process analysis. The atmospheric transport represents the combined contributions of
634 horizontal diffusion (HDIF), horizontal advection (HADV), vertical diffusion (VDIF), and
635 vertical advection (ZADV) in the process analysis. The results indicate that the increase
636 in surface ozone was primarily driven by photochemical reactions. During the period
637 dominated by Typhoon Bavi (August 24-27), photochemical reactions intensified
638 rapidly over Guangdong Province, contributing more than 30 ppbv to surface ozone
639 concentrations in the central region (**Figs. S8a-d**). Under the influence of Typhoon
640 Maysak (August 28-29), the positive contribution from photochemical reactions was
641 slightly lower than in the previous phase, but still exceeded 16 ppbv in the central
642 Guangdong region (**Figs. S8e-f**). The contribution of atmospheric transport varied
643 significantly across different altitudes, exhibiting predominantly negative effects below
644 850 hPa and positive effects above 850 hPa. Vertical cross-sections of daily mean
645 atmospheric transport contributions reveal a gradual southward transport of ozone
646 from higher to lower latitudes. However, its positive contribution to ozone
647 concentrations was substantially lower than that of photochemical reactions, with
648 daily mean contributions remaining below 4.5 ppbv (**Fig. S9**). The downward transport
649 of upper-level ozone inhibited vertical diffusion of surface ozone while simultaneously



650 transporting high-concentration ozone downward into the boundary layer, further
651 intensifying ozone pollution levels. In summary, during this ozone pollution event
652 caused by consecutive northward-moving typhoons: Chemical processes were the
653 main cause of surface ozone pollution in Guangdong Province, Atmospheric transport
654 was a secondary contributing factor.



655
656 Figure 9. Temporal evolution of (a-f) horizontal distributions of surface ozone and (g-l) vertical
657 distributions (along 114°E cross-section) of ozone from 1400 LST 24 August to 1400 LST 29 August
658 2020.

659 To quantitatively analyze the contribution of vertical transport to ozone
660 concentrations within the boundary layer, we employed the IPR (Integrated Process
661 Rate) analysis method to decompose ozone sources and sinks across the study area. A
662 detailed analysis was conducted using results from the Sanshui station at 100m and

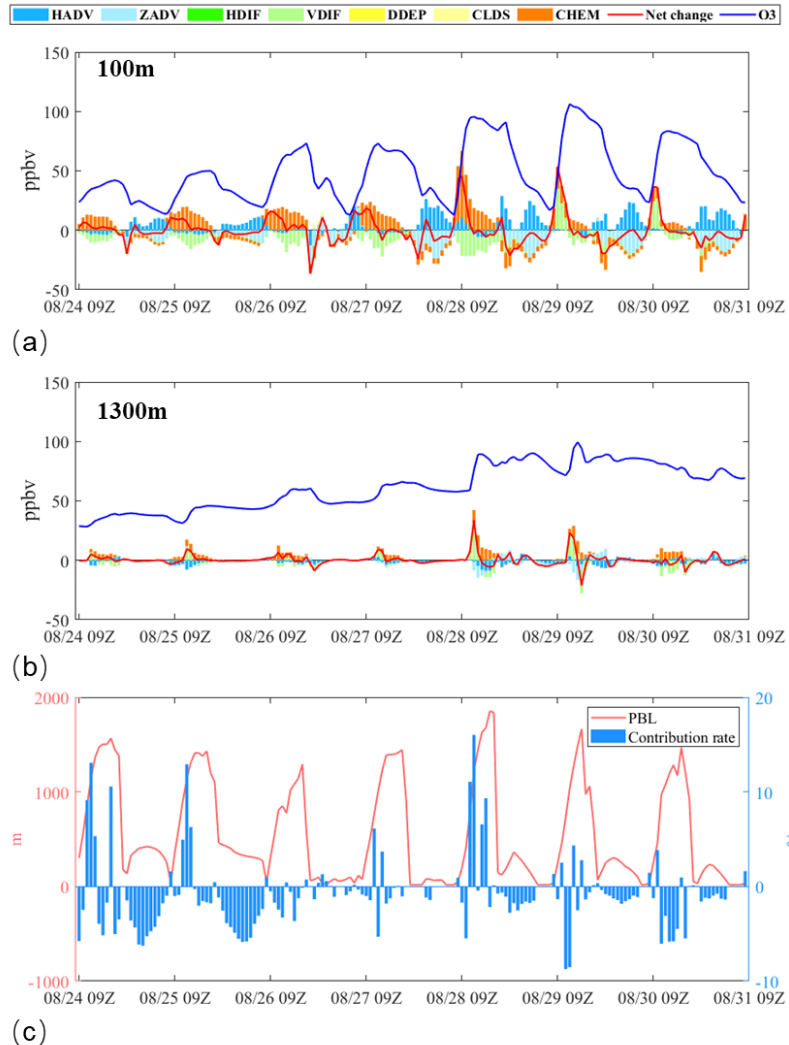


663 1300m altitudes (**Fig.10a-b**). Subsequently, we calculated the contribution rate of
664 cross-boundary-layer vertical transport to ozone concentrations in the boundary layer
665 at each time point (**Fig.10c**) using the following formula (Chen et al., 2022a):

666
$$\text{Transport flux} = (IPR_{v,pbl} \times Z_{pbl}) \div (\sum_{j=1}^{pbl} O_{3,j} \times Z_j) * 100\%$$

667 where $IPR_{v,pbl}$ indicates the IPR value corresponding to vertical transport
668 (VDIF+ZADV) on the Boundary layer height. that is, the change in the values of
669 pollutants caused by the vertical diffusion, Z_{pbl} represents the height of the layer in
670 the model that is close to the height of the boundary layer. $O_{3,j}$ indicates the ozone
671 concentration in layer j , Z_j represents the height of j layer.

672 Detailed analysis of process contributions at different heights within the
673 boundary layer shows that while near-surface atmospheric transport exhibited
674 negative contributions to daily mean ozone concentrations, the decomposition of
675 individual processes at 100m height revealed positive contributions from vertical
676 diffusion (VDIF) during 0900-1100 LST on 29 August, with magnitudes of 39.9 ppbv,
677 26.4 ppbv, and 12.3 ppbv respectively (**Fig. 10a**). Further analysis of process
678 contributions at 1300m height reveals distinct positive signals from vertical transport
679 during the morning hours of both 28 and 29 August (**Fig. 10b**). This confirms that
680 upper-level ozone can be transported into the boundary layer, thereby influencing
681 ozone concentrations within the boundary layer. Calculation of cross-boundary-layer
682 vertical transport contributions revealed six distinct ozone transport events during this
683 consecutive northward-moving typhoon episode, occurring on 24, 25, 27, 28, 29, and
684 30 August. The maximum contribution rate to ozone concentrations within the
685 boundary layer reached 16%.



686

687 Figure 10. Process contributions to ozone concentrations at 100m and 1300m altitudes, and
688 cross-boundary-layer vertical transport contribution rates. (a-b: Contributions from horizontal
689 diffusion (HDIF), horizontal advection (HADV), vertical diffusion (VDIF), vertical advection (ZADV),
690 chemical processes (CHEM), dry deposition (DDEP), and cloud processes (CLDS). c: Red lines
691 indicate net ozone change, while blue lines show ozone concentration variations.)

692 5 Conclusions

693 This study systematically investigated the mechanisms by which different
694 typhoon tracks influence ozone pollution in Guangdong Province through
695 meteorological factors, atmospheric circulation patterns, transport trajectories, and



696 vertical transport contributions, based on 237 typhoons in China's adjacent waters
697 from 2013-2023. The key findings are:

- 698 1. Historical typhoons were classified into three types using the K-MEANS
699 clustering method: westward-moving typhoons (Type 1), distant northward-
700 moving typhoons (Type 2), and proximal northward-recurving typhoons (Type
701 3). Among these, near-track northward-moving typhoons are more likely to
702 induce ozone pollution in Guangdong Province due to their more extreme
703 meteorological conditions, including higher temperatures, stronger solar
704 radiation, lower cloud cover, reduced precipitation, decreased relative
705 humidity, elevated boundary layer height, weaker surface winds, and
706 suppressed vertical motion.
- 707 2. Under the influence of northward-moving typhoons (type2 and type3), an
708 upper-level anticyclonic center forms near the tropopause height in mid-
709 latitudes, causing the westerly jet stream to shift southward. This process
710 triggers the subsidence of high-concentration ozone from the upper
711 troposphere, accompanied by pole-to-equator transport. Comparative
712 analysis between typhoon and non-typhoon conditions reveals that both
713 types of northward-moving typhoons induce significant ozone enhancement
714 throughout the vertical column, with increases ranging from 2.5 to 11.6 ppbv
715 (Type 2) and 0.3 to 12.3 ppbv (Type 3).
- 716 3. For Type 1 typhoons, the associated ozone pollution is primarily controlled by
717 the radiative high-pressure system, with significant contributions from local
718 pollution sources. In contrast, Type 2 and Type 3 typhoons exhibit the highest
719 proportions of upper-level transport trajectories (23.9% and 15.2%,
720 respectively), capable of delivering air masses from as high as 9,980 m (~250
721 hPa) into the boundary layer. Coupled with the elevated ozone concentrations
722 along these transport pathways, these mechanisms result in ozone
723 enhancements of 10.7 ppbv and 12.3 ppbv at boundary layer altitudes for



724 Type 2 and Type 3, respectively.

725 4. Under the influence of two consecutive northward-moving typhoons from
726 August 21 to September 6, 2020, Guangdong Province experienced a
727 prolonged ozone pollution episode. On August 29, ozone exceedance was
728 observed at 54.3% of monitoring stations. The primary cause of this ozone
729 pollution event was enhanced photochemical production, with secondary
730 contributions from upper-level ozone transport. Process analysis revealed
731 that during 09:00-11:00 LST on August 29, the positive contributions of near-
732 surface vertical transport to ozone concentrations were 39.9 ppbv, 26.4 ppbv,
733 and 12.3 ppbv, respectively. During this typhoon event, cross-boundary-layer
734 transport via vertical mixing contributed up to 16% of the ozone
735 concentration within the boundary layer.

736

737

738 **Acknowledgments**

739 The text ends with an acknowledgment section and statement that includes:

740 • National Natural Science Foundation of China (42121004, 42477273 and
741 42405194)
742 • Guangdong Basic and Applied Basic Research Foundation (2023A1515110103 and
743 2024A1515510025)
744 • Science and Technology Planning Project of Guangzhou (2025A04J4711)
745 • Guangdong Province: Special Support Plan for High-Level Talents (2023JC07L057)
746 • Guangdong Provincial General Colleges and Universities Innovation Team Project
747 (Natural Science, 2024KCXTD004)

748

749 **References**

750 Chen, X., Liu, Y., Lai, A., Han, S., Fan, Q., Wang, X., Ling, Z., Huang, F., and Fan, S.:



751 Factors dominating 3-dimensional ozone distribution during high tropospheric ozone
752 period, *Environ. Pollut.*, 232, 55–64, <https://doi.org/10.1016/j.envpol.2017.09.017>,
753 2018.

754 Chen, X., Wu, L., Chen, X., Zhang, Y., Guo, J., Safieddine, S., Huang, F., and Wang, X.:
755 Cross-Tropopause Transport of Surface Pollutants during the Beijing 21 July Deep
756 Convection Event, *J. Atmos. Sci.*, 79, 1349–1362, <https://doi.org/10.1175/JAS-D-21-0115.1>, 2022a.

757 Chen, X., Wang, N., Wang, G., Wang, Z., Chen, H., Cheng, C., Li, M., Zheng, L., Wu, L.,
758 Zhang, Q., Tang, M., Huang, B., Wang, X., and Zhou, Z.: The Influence of Synoptic
759 Weather Patterns on Spatiotemporal Characteristics of Ozone Pollution Across Pearl
760 River Delta of Southern China, *J. Geophys. Res. Atmos.*, 127, 1–17,
761 <https://doi.org/10.1029/2022jd037121>, 2022b.

762 Chen, Y., Lu, X., and Fung, J. C. H.: Spatiotemporal source apportionment of ozone
763 pollution over the Greater Bay Area, *Atmos. Chem. Phys.*, 24, 8847–8864,
764 <https://doi.org/10.5194/acp-24-8847-2024>, 2024.

765 Chen, Z., Liu, J., Cheng, X., Yang, M., and Wang, H.: Positive and negative influences
766 of typhoons on tropospheric ozone over southern China, *Atmos. Chem. Phys.*, 21,
767 16911–16923, <https://doi.org/10.5194/acp-21-16911-2021>, 2021.

768 Chen, Z., Liu, J., Qie, X., Cheng, X., Shen, Y., Yang, M., Jiang, R., and Liu, X.: Transport
769 of substantial stratospheric ozone to the surface by a dying typhoon and shallow
770 convection, *Atmos. Chem. Phys.*, 22, 8221–8240, <https://doi.org/10.5194/acp-22-8221-2022>, 2022c.

771 Cong, H., Yuan, Y., Qian, W., and Bi-hui, Z.: Analysis of O3 Pollution Affected by a
772 Succession of Three Landfall Typhoons in 2020 in Eastern China, *Huanjing Kexue*, 45,
773 71–80, <https://doi.org/10.13227/j.hjkx.202301049>, 2024.

774 Ding, H., Kong, L., You, Y., Mao, J., Chen, W., Chen, D., Chang, M., and Wang, X.:
775 Effects of tropical cyclones with different tracks on ozone pollution over the Pearl
776 River Delta region, *Atmos. Res.*, 286,
777 <https://doi.org/10.1016/j.atmosres.2023.106680>, 2023.

778 Dou, X., Li, M., Jiang, Y., Song, Z., Li, P., and Yu, S.: Different contributions of
779 meteorological conditions and emission reductions to the ozone pollution during
780 Shanghai's COVID-19 lockdowns in winter and spring, *Atmos. Pollut. Res.*, 15,
781 <https://doi.org/10.1016/j.apr.2024.102252>, 2024.

782 Gao, D., Xie, M., Chen, X., Wang, T., Liu, J., Xu, Q., Mu, X., Chen, F., Li, S., Zhuang, B.,
783 Li, M., Zhao, M., and Ren, J.: Systematic classification of circulation patterns and
784 integrated analysis of their effects on different ozone pollution levels in the Yangtze
785 River Delta Region, China, *Atmos. Environ.*, 242,
786 <https://doi.org/10.1016/j.atmosenv.2020.117760>, 2020.

787 Gong, D., Du, N., Wang, L., Deng, X., Zhang, X., and Yang, L.: Impacts of
788 meteorological and precursor emission factors on PM2.5 and O3 from 2019 to 2022:
789 Insights from multiple perspectives, *Atmos. Res.*, 315,
790 <https://doi.org/10.1016/j.atmosres.2025.107933>, 2025.



793 Guo, Y. P. and Tan, Z. M.: Influence of Track Change on the Inconsistent Poleward
794 Migration of Typhoon Activity, *J. Geophys. Res. Atmos.*, 127, 1–16,
795 <https://doi.org/10.1029/2022JD036640>, 2022.

796 Han, H., Liu, J., Shu, L., Wang, T., and Yuan, H.: Local and synoptic meteorological
797 influences on daily variability in summertime surface ozone in eastern China, *Atmos.*
798 *Chem. Phys.*, 20, 203–222, <https://doi.org/10.5194/acp-20-203-2020>, 2020a.

799 Han, H., Liu, J., Shu, L., Wang, T., and Yuan, H.: Local and synoptic meteorological
800 influences on daily variability in summertime surface ozone in eastern China, *Atmos.*
801 *Chem. Phys.*, 20, 203–222, <https://doi.org/10.5194/acp-20-203-2020>, 2020b.

802 Hu, F., Xie, P., Zhu, Y., Zhang, F., Xu, J., Lv, Y., Zhang, Z., Zheng, J., Zhang, Q., Li, Y.,
803 and Tian, X.: The impact of evolving synoptic weather patterns on multi-scale
804 transport and sources of persistent high-concentration ozone pollution event in the
805 Yangtze River Delta, China, *Sci. Total Environ.*, 949,
806 <https://doi.org/10.1016/j.scitotenv.2024.175048>, 2024.

807 Huang, D., Wan, L., Wan, Y., Chang, S., Ma, X., and Zhao, K.: Gravity Wave Activity
808 and Stratosphere-Troposphere Exchange During Typhoon Molave (2020), *J. Trop.*
809 *Meteorol.*, 30, 306–326, <https://doi.org/10.3724/j.1006-8775.2024.026>, 2024.

810 Huang, T., Yang, Y., O'Connor, E. J., Lolli, S., Haywood, J., Osborne, M., Cheng, J. C.-H.,
811 Guo, J., and Yim, S. H.-L.: Influence of a weak typhoon on the vertical distribution of
812 air pollution in Hong Kong: A perspective from a Doppler LiDAR network, *Environ.*
813 *Pollut.*, 276, <https://doi.org/10.1016/j.envpol.2021.116534>, 2021.

814 Jiang, Y., Zhao, T., Meng, K., Cheng, X., and Lv, Q.: 3-D Changes of Tropospheric O₃ in
815 Central and Eastern China Induced by Tropical Cyclones over the Northwest Pacific:
816 Recent-Year Characterization with Multi-Source Observations, *Remote Sens.*, 16,
817 <https://doi.org/10.3390/rs16071178>, 2024.

818 Kumar, S., Chen, W., and Louis, O.-P.: Ionospheric and Atmospheric Response to
819 Extremely Severe Cyclonic Storm Nida of 29 July-02 August 2016, *J. Geophys. Res.*
820 *Phys.*, 128, <https://doi.org/10.1029/2023JA031422>, 2023.

821 Li, D., Vogel, B., Mueller, R., Bian, J., Guenther, G., and Riese, M.: Tropical Cyclones
822 Reduce Ozone in the Tropopause Region Over the Western Pacific: An Analysis of 18
823 Years Ozonesonde Profiles, *EARTHS Futur.*, 9,
824 <https://doi.org/10.1029/2020EF001635>, 2021.

825 Li, D., Bian, J., Zhang, X., Vogel, B., Muller, R., and Gunther, G.: Impact of typhoon
826 Soudelor on ozone and water vapor in the Asian monsoon anticyclone western
827 Pacific mode, *Atmos. Sci. Lett.*, 24, <https://doi.org/10.1002/asl.1147>, 2023a.

828 Li, M., Zeng, W., Yang, Z., Luo, Y., Zhu, Q., Wang, L., Yang, L., and Liao, C.: Multiple
829 sources emission inventory closely integrated with atmospheric environment
830 management: A case study of Guangdong, China, *Atmos. Pollut. Res.*, 14, 101825,
831 <https://doi.org/10.1016/j.apr.2023.101825>, 2023b.

832 Li, Y., Zhao, X., Deng, X., and Gao, J.: The impact of peripheral circulation
833 characteristics of typhoon on sustained ozone episodes over the Pearl River Delta
834 region, China, *Atmos. Chem. Phys.*, 22, 3861–3873, <https://doi.org/10.5194/acp-22->



835 3861-2022, 2022.

836 Lu, P., Liu, R., Luo, Z., Li, S., Wu, Y., Hu, W., and Xue, X.: Impacts of compound
837 extreme weather events on summer ozone in the Beijing-Tianjin-Hebei region,
838 *Atmos. Pollut. Res.*, 15, <https://doi.org/10.1016/j.apr.2023.102030>, 2024.

839 Lu, X., Yu, H., Ying, M., Zhao, B., Zhang, S., Lin, L., Bai, L., and Wan, R.: Western North
840 Pacific Tropical Cyclone Database Created by the China Meteorological
841 Administration, *Adv. Atmos. Sci.*, 38, 690–699, <https://doi.org/10.1007/s00376-020-0211-7>, 2021.

842 Ouyang, S., Deng, T., Liu, R., Chen, J., He, G., Leung, J. C.-H., Wang, N., and Liu, S. C.:
843 Impact of a subtropical high and a typhoon on a severe ozone pollution episode in
844 the Pearl River Delta, China, *Atmos. Chem. Phys.*, 22, 10751–10767,
845 <https://doi.org/10.5194/acp-22-10751-2022>, 2022.

846 Qin, L., Chunyan, D., Biwu, C., and Jianfeng, L.: Reason Analysis and Control of Ozone
847 Pollution in a Southern Coastal City, 2020.

848 Qiu, Y., Li, X., Chai, W., Liu, Y., Song, M., Tian, X., and Zou, Q.: Insights into ozone
849 pollution control in urban areas by decoupling meteorological factors based on
850 machine learning, 2013, 1749–1763, 2025.

851 Qu, K., Wang, X., Yan, Y., Shen, J., Xiao, T., Dong, H., Zeng, L., and Zhang, Y.: A
852 comparative study to reveal the influence of typhoons on the transport, production
853 and accumulation of O₃ in the Pearl River Delta, China, *Atmos. Chem. Phys.*, 21,
854 11593–11612, <https://doi.org/10.5194/acp-21-11593-2021>, 2021.

855 Rolph, G., Stein, A., and Stunder, B.: Real-time Environmental Applications and
856 Display sYstem: READY, *Environ. Model. Softw.*, 95, 210–228,
857 <https://doi.org/10.1016/j.envsoft.2017.06.025>, 2017.

858 Shen, W., Jin, Y., Li, G., and Cong, P.: Analyzing the response distribution of DO
859 concentration and its environmental factors under the influence of typhoon rain
860 events with remote sensing, *Front. Ecol. Evol.*, 11,
861 <https://doi.org/10.3389/fevo.2023.1283281>, 2023.

862 Shuping, S., Chen, C., Haihua, M., Zhuoran, H., Lina, A., Sixin, D., Yan, Z., Min'er, K.,
863 and Weihua, C.: Characteristics of ozone pollution in Foshan city and its relationship
864 with meteorology during 2017-2019, 2022.

865 Stein, A. F., Draxler, R. R., Rolph, G. D., Stunder, B. J. B., Cohen, M. D., and Ngan, F.:
866 Noaa's hysplit atmospheric transport and dispersion modeling system, *Bull. Am.*
867 *Meteorol. Soc.*, 96, 2059–2077, <https://doi.org/10.1175/BAMS-D-14-00110.1>, 2015.

868 Wan, Y., Yin, Z., Huo, Q., Zhou, B., and Wang, H.: Weather Extremes Led to Large
869 Variability in O₃ Pollution and Associated Premature Deaths in East of China, *Front.*
870 *EARTH Sci.*, 10, <https://doi.org/10.3389/feart.2022.947001>, 2022.

871 Wang, J., Wang, P., Tian, C., Gao, M., Cheng, T., and Mei, W.: Consecutive Northward
872 Super Typhoons Induced Extreme Ozone Pollution Events in Eastern China, *npj Clim.*
873 *Atmos. Sci.*, 7, 1–9, <https://doi.org/10.1038/s41612-024-00786-z>, 2024a.

874 Wang, J., Wang, P., Tian, C., Gao, M., Cheng, T., and Mei, W.: Consecutive Northward
875 Super Typhoons Induced Extreme Ozone Pollution Events in Eastern China, *NPJ Clim.*
876



877 Atmos. Sci., 7, <https://doi.org/10.1038/s41612-024-00786-z>, 2024b.

878 Wang, K., Zhao, R., Wu, Q., Li, J., Wang, H., and Lin, H.: Responses of surface ozone
879 under the tropical cyclone circulations: Case studies from Fujian Province, China,
880 Atmos. Pollut. Res., 16, <https://doi.org/10.1016/j.apr.2024.102323>, 2025.

881 Wang, N., Ling, Z., Deng, X., Deng, T., Lyu, X., Li, T., Gao, X., and Chen, X.: Source
882 Contributions to PM2.5 under Unfavorable Weather Conditions in Guangzhou City,
883 China, Adv. Atmos. Sci., 35, 1145–1159, <https://doi.org/10.1007/s00376-018-7212-9>,
884 2018.

885 Wang, N., Huang, X., Xu, J., Wang, T., Tan, Z. M., and Ding, A.: Typhoon-boosted
886 biogenic emission aggravates cross-regional ozone pollution in China, Sci. Adv., 8,
887 <https://doi.org/10.1126/sciadv.abl6166>, 2022a.

888 Wang, N., Huang, X., Xu, J., Wang, T., Tan, Z. M., and Ding, A.: Typhoon-boosted
889 biogenic emission aggravates cross-regional ozone pollution in China, Sci. Adv., 8, 1–
890 8, <https://doi.org/10.1126/sciadv.abl6166>, 2022b.

891 Wang, N., Wang, H., Huang, X., Chen, X., Zou, Y., Deng, T., Li, T., Lyu, X., and Yang, F.:
892 Extreme weather exacerbates ozone pollution in the Pearl River Delta, China: role of
893 natural processes, Atmos. Chem. Phys., 24, 1559–1570, <https://doi.org/10.5194/acp-24-1559-2024>, 2024c.

894 Wei, J., Li, Z., Li, K., Dickerson, R. R., Pinker, R. T., Wang, J., Liu, X., Sun, L., Xue, W.,
895 and Cribb, M.: Full-coverage mapping and spatiotemporal variations of ground-level
896 ozone (O₃) pollution from 2013 to 2020 across China, Remote Sens. Environ., 270,
897 <https://doi.org/10.1016/j.rse.2021.112775>, 2022.

898 Xu, J., Zhou, D., Gao, J., Huang, X., Xue, L., Huo, J., Fu, Q., and Ding, A.: Biogenic
899 emissions-related ozone enhancement in two major city clusters during a typical
900 typhoon process, Appl. GEOCHEMISTRY, 152,
901 <https://doi.org/10.1016/j.apgeochem.2023.105634>, 2023.

902 Yang, L., Luo, H., Yuan, Z., Zheng, J., Huang, Z., Li, C., Lin, X., K K Louie, P., Chen, D.,
903 and Bian, Y.: Quantitative impacts of meteorology and precursor emission changes
904 on the long-term trend of ambient ozone over the Pearl River Delta, China, and
905 implications for ozone control strategy, Atmos. Chem. Phys., 19, 12901–12916,
906 <https://doi.org/10.5194/acp-19-12901-2019>, 2019.

907 Yaoyao, C., Tong, L., Yu, W., Jin, S., Yuhong, Z., Siqi, Y., Duohong, C., and Jingyang, C.:
908 Characteristics of Ozone Pollution in Guangdong Province from 2016 to 2020, 2022.

909 Ying, M., Zhang, W., Yu, H., Lu, X., Feng, J., Fan, Y., Zhu, Y., and Chen, D.: An Overview
910 of the China Meteorological Administration Tropical Cyclone Database, J. Atmos.
911 Ocean. Technol., 31, 287–301, <https://doi.org/https://doi.org/10.1175/JTECH-D-12-00119.1>, 2014.

912 Yufeng, Z., Junjun, Y., Tingting, C., Tao, W., Huang, C., Lili, Z., Boguang, W., and
913 Chengliang, Z.: Influence of typhoon track in northwest Pacific on ozone pollution in
914 autumn in Shantou City, 2024.

915 Zhan, C., Xie, M., Huang, C., Liu, J., Wang, T., Xu, M., Ma, C., Yu, J., Jiao, Y., Li, M., Li,
916 S., Zhuang, B., Zhao, M., and Nie, D.: Ozone affected by a succession of four landfall



919 typhoons in the Yangtze River Delta, China: major processes and health impacts,
920 Atmos. Chem. Phys., 20, 13781–13799, <https://doi.org/10.5194/acp-20-13781-2020>,
921 2020.

922 Zhu, L., Zhou, R., Di, D., Bai, W., and Liu, Z.: Retrieval of Atmospheric Water Vapor
923 Content in the Environment from AHI/H8 Using Both Physical and Random Forest
924 Methods-A Case Study for Typhoon Maria (201808), Remote Sens., 15,
925 <https://doi.org/10.3390/rs15020498>, 2023.

926

927

928